# Langmuir turbulence and three-wave nonlinear dynamics

S. E. Gibson, D. L. Newman, and M. V. Goldman
*Astrophysical Planetary and Atmospheric Sciences Department, University of Colorado at Boulder, Campus Box 391, Boulder, Colorado 80309-0391*
(Received 9 February 1995)

The parametric decay of a single linearly unstable Langmuir wave into broad spectra of damped daughter Langmuir and ion-acoustic waves is studied by means of the Zakharov partial differential equations in one dimension. In the regime investigated, the multimode daughter wave spectra are found to exhibit locked-in-time behavior, allowing a reduction to an equivalent three-mode system. The dynamics of the reduced system are found to be in quantitative agreement with those of the multimode Zakharov simulations. Qualitative agreement is maintained when the ion-acoustic response is reduced from second order to first order. The nonlinear dynamics of the resulting (complex) third-order system are studied analytically and numerically with emphasis on cases when the daughter modes are unequally damped. The special case of exact linear frequency matching between the pump and daughter modes is also considered.

PACS number(s): 03.40.Gc, 52.35.Mw, 02.60.Cb, 52.35.Ra

## I. INTRODUCTION

In continuous media, such as plasmas and fluids, the fundamental dynamics of nonlinear disturbances are usually described by systems of partial differential equations (PDE's). Galerkin expansions and truncations to a few normal modes are commonly used to reduce the number of degrees of freedom of the systems to a very low order. A great deal of attention has been paid to the nonlinear dynamics of three- and four-mode systems [1–3], but the relevance to "real" physical systems (as represented by PDE's) has not always been clear.

The purpose of this paper is threefold.

(1) To numerically study the one-dimensional (1D) driven Zakharov PDE system, which is capable of representing a turbulent state consisting of many coupled waves, in a regime where an unstable monochromatic "pump" wave is parametrically coupled to two daughter multimode wave spectra.

(2) To reduce this PDE system to an equivalent dynamical system of three coupled waves that exhibit the same nonlinear dynamics as the larger (PDE) system in the regimes studied.

(3) To further study the nonlinear dynamics of this generalized three-wave system.

We begin with a discussion of the two-time-scale Zakharov [4] PDE model of the nonlinear interactions of electron plasma (Langmuir) waves and ion-acoustic waves. Similar equations have been employed extensively to analyze turbulence in various other systems [3,5]. In particular, we study a system where an unstable "pump" Langmuir wave drives two daughter waves: one Langmuir and one ion-acoustic. Parameters for our one-dimensional studies are motivated by a recent 2D Zakharov-equation analysis [6–8] of electron-beam-driven Langmuir turbulence detected by sounding rockets in the Earth's magnetized auroral ionosphere. In order to simplify the problem and make contact with three-wave models, the system is assumed to be driven by a single unstable pump Langmuir wave, with resonant phase velocity and temporal growth rates due to the putative auroral electron beam. All other Langmuir-wave modes are damped in $k$ space with a power-law damping rate inferred from measured (approximately isotropic) power-law tails on the electron distributions.

Numerical solutions to the driven Zakharov equations are found in a parameter regime where the dominant nonlinear behavior is the single backscatter of the beam-unstable mode off ion-acoustic waves. This regime, in which there is heavy daughter Langmuir-wave damping and/or a weakly unstable pump, differs from the multiple-backscatter or "cascade" regime characterized by stronger pumps and weaker damping. In the case we study, backscatter decay typically removes Langmuir-wave energy from modes resonant with the beam electrons and can therefore saturate the instability. However, in the fully nonlinear states discussed here, energy will sometimes flow from the daughter modes back to the beam-resonant mode. These wave-wave processes are assumed to dominate resonant-wave backreaction on the beam (i.e., quasilinear effects). Although the pump consists of a single $k$-space mode, the daughter waves (both Langmuir and ion-acoustic) are composed of a large number of modes, which contribute to fairly narrow spectral *packets* centered near the nominal wave numbers for three-wave backscatter decay. The *frequency* spectrum of the daughter Langmuir waves is, nevertheless, dominated by a single frequency that has a linear correspondence to a single (mean) wave number of the packet along with sideband frequencies representative of nonlinear processes. The time history of the total wave energy exhibits either limit-cycle behavior or chaotic behavior, depending on the ratio of the growth rate of the beam-resonant mode to the damping rate of a typical backscattered Langmuir wave.

An examination of the wave number spectra during the nonlinear evolution of the system reveals strong phase

1063-651X/95/52(1)/558(14)/$06.00

correlations between the daughter Langmuir and ion-acoustic waves. These observed correlations are the basis for a reduction of the PDE system to a simpler three-mode system in which the daughter Langmuir and ion-acoustic spectral packets are each treated as a single *equivalent lumped mode.* The mismatch $\Delta$ between the pump-wave frequency and the sum of the *mean* linear frequencies of the two daughter modes is determined by the details of the Zakharov simulations, but is left as a free parameter in the reduced three-wave system.

Following a further simplification, in which the ion-acoustic response is reduced from second to first order, the three-wave system described here can be regarded as a generalization of a system studied by Wersinger, Finn, and Ott [9] (hereafter, WFO). WFO considered the interaction between a linearly unstable wave and two identically damped lower-frequency daughter waves. By varying the single damping rate, they observed an evolution in the system's dynamics from periodic limit cycles through bifurcations into chaos. Their assumption of identical damping for the daughter waves reduced the dynamical system to three real degrees of freedom. A by-product of this assumption was that in the limit of zero linear frequency mismatch between the pump and daughter waves ($\Delta = 0$) the dynamics became unstable and solutions became unbounded.

Our analysis extends the work of WFO by permitting the damping rates of the two daughter waves to differ from one another. Since in our case one of the daughter waves will be a Langmuir wave and the other an ion-acoustic wave, a restriction to equal damping rates cannot be justified on physical grounds. Allowing different damping rates increases the dimension of the dynamical system from three to four (real) degrees of freedom. The nonlinear behavior exhibited by the four-dimensional system generally differs from that of the three-dimensional one studied by WFO. One consequence of our generalization is that the condition $\Delta = 0$ no longer leads to unstable dynamics. This special limit of zero frequency mismatch, which we consider here, also leads to a reduction of the system to three dimensions; however, this reduced system is different from the one studied by WFO.

The structure of the remainder of this paper is as follows: In Sec. II we discuss the Zakharov PDE model of the nonlinear coupling of Langmuir and ion-acoustic waves. We also describe the driving and dissipation parameters used in our numerical solutions of the Zakharov equations—as discussed above these parameters are based on recent [6–8] two-dimensional auroral magnetized plasma studies. A brief discussion of the numerical codes is also provided. Specific numerical solutions of the Zakharov equations are presented in Sec. III, along with an analysis of the nonlinear wave number spectra. In Sec. IV we derive a reduced three-coupled-wave system directly from the Zakharov equations under constraints determined from the numerical solutions. Section V contains a comparison of Zakharov-equation dynamics with the dynamics of the reduced three-wave system with lumped-mode parameters determined from the Zakharov spectra. The reduced three-wave system is next examined analytically in Sec. VI in order to delineate features of the general four-dimensional dynamics such as fixed point stability and four-space volume contraction. A numerical study of the system dynamics over a wide range of parameters is presented in Sec. VII in both the general four-dimensional regime as well as in the special three-dimensional limit associated with zero frequency mismatch. Finally, Sec. VIII contains concluding remarks.

## II. PARTIAL DIFFERENTIAL EQUATION MODEL

### A. Zakharov-equation description of wave interactions

The electrostatic Zakharov equations [4] describe the nonlinear coupling between Langmuir waves and ion-acoustic waves (not including the effects of wave-particle nonlinearities). The dimensionless Zakharov equations in a multidimensional unmagnetized plasma can be written as

$$\boldsymbol{\nabla}\cdot(i\partial_t + i\hat{\gamma} + \boldsymbol{\nabla}^2)\mathbf{E}(\mathbf{x},t) = \boldsymbol{\nabla}\cdot(\delta n\mathbf{E}), \tag{1a}$$

$$(\partial_t^2 + 2\hat{\gamma}_{ia}\partial_t - \nabla^2)\delta n(\mathbf{x},t) = \nabla^2|\mathbf{E}|^2. \tag{1b}$$

The Langmuir electric field *envelope* $\mathbf{E}$ is related to the high-frequency electric field $\mathcal{E}$ through the relation $\mathcal{E} = \mathrm{Re}(\mathbf{E}e^{-i\omega_e t})$. The low-frequency quasineutral density perturbation is $\delta n$ and the Langmuir and ion-acoustic damping operators (whose Fourier transforms are the $k$-space damping rates) are $\hat{\gamma}$ and $\hat{\gamma}_{ia}$, respectively.

The units used in Eqs. (1a) and (1b) are such that the following replacements yield physical units:

$$t \to \frac{2}{3}\frac{m_e}{m_i}\omega_e t, \quad \boldsymbol{\nabla} \to \tfrac{3}{2}\sqrt{m_i/m_e}\lambda_e\boldsymbol{\nabla},$$

$$\delta n \to \frac{3}{2}\frac{m_i}{m_e}\frac{\delta n}{n_0}, \quad E^2 \to \frac{3}{4}\frac{m_i}{m_e}\frac{E^2}{16\pi n_0 T_e},$$

where

$$\omega_e = \frac{4\pi n_0 e^2}{m_e}, \quad \lambda_e = \frac{\sqrt{T_e/m_e}}{\omega_e}$$

are the electron plasma frequency and electron Debye length, respectively. The parameters $m_e$, $m_i$, and $T_e$ are the electron and ion mass and the electron temperature, and $n_0$ is the mean electron number density.

The first Zakharov equation describes the evolution of the slowly varying envelope of a Langmuir-wave electric field. The linear evolution of the envelope is described by the left side of Eq. (1a) and the nonlinear effects of the density perturbations (which cause Langmuir waves to refract into low-density regions) are contained on the right side. Equation (1b) describes the linear evolution of ion-acoustic waves (left) driven by the nonlinear ponderomotive force of Langmuir waves (right).

As written, the Zakharov equations are valid in a multiple dimensional system where $\mathbf{E} = -\boldsymbol{\nabla}\phi$ for a scalar potential $\phi$. Henceforth, we consider only a 1D system. Thus, the electrostatic field itself will be a scalar $E$ and

the divergence operating on both the left and right sides of (1) become superfluous.

Upon taking the Fourier transforms of the 1D reductions of (1a) and (1b), the Zakharov equations can be written in their $k$-space representation,

$$[i\partial_t + i\gamma(k) - k^2]E_k(t) = \sum_q \delta n_q(t) E_{k-q}(t), \tag{2a}$$

$$[\partial_t^2 + 2\gamma_{ia}(k)\partial_t + k^2]\delta n_k(t) = -k^2 \sum_q E_q(t)[E^*(t)]_{k-q}, \tag{2b}$$

where we use subscripts instead of functional notation for the wave number dependence of the fields to distinguish them from the corresponding real-space quantities. The summations on the right sides of (2a) and (2b) are the discrete convolutions corresponding to the products of fields on the right sides of (1a) and (1b). Here $\gamma(k)$ and $\gamma_{ia}(k)$ are the Langmuir and ion-acoustic damping rates, which are related to the damping operators $\hat{\gamma}$ and $\hat{\gamma}_{ia}$ in (1a) and (1b) through a Fourier transform.

### B. Application to beam-driven Langmuir turbulence in the auroral zone

The Zakharov equations have been the basis of a number of numerical studies of Langmuir turbulence driven by electron beams [10–12]. A sufficiently intense electron beam with velocity $v_b$ will linearly destabilize Langmuir waves with a phase velocity slightly below $v_b$ (i.e., waves resonant with the positive slope on the distribution function). Thus, Langmuir waves with $k = k_b \gtrsim \omega_e/v_b$ will be unstable with growth rate $\gamma(k_b) < 0$ (i.e., negative damping).

Under conditions where wave-particle nonlinearities, which can modify the electron distribution, are sufficiently slow, the Langmuir waves at $k_b$ will grow until they exceed the threshold for the *backscatter decay* instability. Backscatter decay is a resonant three-wave interaction that transfers energy from unstable Langmuir waves at $k_b$ into backward propagating Langmuir waves at $k_S = -k_b + k_*$ and ion-acoustic waves at $k_{ia} = 2k_b - k_*$. Here, $k_*\lambda_e = (2c_s/3v_e)$, where $c_s = (m_e/m_i)^{1/2}v_e$ is the ion-sound speed and $v_e$ is the electron thermal velocity. Thus, backscatter decay is a nonlinear wave-wave interaction that can saturate the linear beam-driven instability. We use the subscript $S$ for the daughter Langmuir wave to indicate that it is a (frequency-downshifted) *Stokes* wave. The (frequency-upshifted) *anti Stokes* wave at wave number $k_A = k_b + k_{ia}$ is far off resonance and plays an insignificant role in the wave-coupling dynamics.

If the plasma is weakly damped at wave numbers below $k_b$ (for example, beam-driven turbulence in the solar wind [12]), the backscattered daughter Langmuir wave can in turn grow to the point where it exceeds the threshold for a second backscatter decay. Multiple backscatter decays are referred to as *backscatter cascade*, which can take Langmuir energy to small wave numbers where it can then couple efficiently to localized wave packets that self-focus and collapse—a coherent-phase regime known as *strong Langmuir turbulence* [13,14].

If the rate of damping of backscattered Langmuir waves is sufficient, the backscatter cascade will cease after at most one or two steps. This situation was investigated [15] for the case where the beam-unstable region of $k$ space contained a large number of phase-incoherent modes. It was found that the energy in the beam-resonant modes and the daughter Langmuir and ion-acoustic modes underwent oscillations that could be described by a Lotka-Voltera system, which is appropriate for three phase-incoherent coupled waves (i.e., *weak Langmuir turbulence*).

In the present study, we consider the contrasting case where only a single beam-resonant mode is excited [16]. The values of simulation parameters used in the numerical study of Sec. III are chosen to model typical conditions in the Earth's auroral ionosphere at the time of intense Langmuir-wave bursts observed by sounding rockets [17,18]. The electron distribution is characterized by an approximately isotropic tail of nonthermal electrons that can be modeled by a power law in velocity [19]. In addition, there are (downward-going) beamlike electrons, aligned with the Earth's magnetic field, that are responsible for destabilizing resonant Langmuir waves. Our 1D model corresponds to wave motions along the geomagnetic field.

Nominal values of the plasma parameters used in the Zakharov equation simulations are presented in Table I. The parameters relating to the ion-acoustic dispersion ($c_s$ and $\gamma_{ia}$) are based on an oxygen plasma with the electron temperature $T_e$ several times the ion temperature $T_i$ (the ion thermal correction to the sound speed has not been included). The only parameter in Table I that takes on different values in the numerical simulations of Sec. III is the Langmuir damping $\gamma(k \neq k_b)$. Specifically, the numerical coefficient $C$ was varied over a range bracketing the nominal value $C = 10$ estimated from measured auroral electron distributions. In the two simulation runs discussed in Sec. III, we use the respective values $C = 12.5$ and $C = 6.25$.

Because the numerical simulations described in this paper are restricted to one dimension, magnetic corrections to the Langmuir dispersion relation do not enter. As discussed in Refs. [6,8], auroral Langmuir turbulence is observed at altitudes where the electron cyclotron frequency $\Omega_e$ is comparable to $\omega_e$, resulting in significant dispersive corrections for waves oblique to the magnetic field. These dispersive corrections have the effect of confining Langmuir waves to a narrow cone about the direction of the magnetic field (i.e., a quasi-1D spectrum). Full 2D simulations with a single pump mode, however,

TABLE I. Nominal plasma parameters.

| $k_b$ | $\gamma(k_b)$ | $\gamma(k \neq k_b)$ | $c_s$ | $\gamma_{ia}(k)$ |
|---|---|---|---|---|
| $0.04\lambda_e^{-1}$ | $-10^{-4}\omega_e$ | $C(k\lambda_e)^3\omega_e$ | $5.8 \times 10^{-3}v_e$ | $0.2kc_s$ |

are not treated in this paper, but are deferred for future study.

### C. Numerical simulation methodology

The Zakharov-equation simulation code used in the present study is a one-dimensional reduction of the multidimensional code described elsewhere [20,21]. The Zakharov equations are solved on a periodic grid of 8192 points. In the $k$-space representation, the grid covers the domain $-0.16 < k\lambda_e \leq 0.16 = k_{\max}\lambda_e$. Thus, the beam-unstable mode $k_b$ (from Table I) is at $k_{\max}/4$. This choice ensures that the ion-acoustic decay mode (at $\sim 2k_b$) is immune to corruption by aliasing.

The grid spacing in $k$ space is $\Delta k = 3.9 \times 10^{-5}\lambda_e^{-1}$. This corresponds to a frequency spacing $\Delta\omega = v_g\Delta k = 4.7 \times 10^{-6}\omega_e$ when evaluated at $k = k_b$. Here, $v_g$ is the Langmuir group velocity $v_g \equiv d\omega/dk \approx 3k\lambda_e^2\omega_e$. This frequency spacing $\Delta\omega$ is small compared to all relevant linear frequencies in the equations (e.g., $\gamma$, $\gamma_{ia}$, etc.), indicating that a sufficiently fine $k$-space grid has been chosen. (Equivalently, the length of the simulation box in physical space $L = \pi/\Delta k$ is sufficiently large.) This claim is validated in the numerical simulations of Sec. III where $\sim 10^2$ daughter modes are excited.

Initial conditions are specified by imposing a uniform, randomly phased distribution of Langmuir waves in $k$ space (i.e., white noise). No initial noise is present in the density perturbations $\delta n$. However, density waves are rapidly driven by the beating of the Langmuir waves. There is no spontaneous emission term in Eq. (1a) to maintain the initial noise level; thus, the Langmuir waves will decay at a rate given by $\gamma(k)$ except for those wave numbers which are fed by the decay of the beam-driven mode.

## III. RESULTS OF ZAKHAROV-EQUATION SIMULATIONS

### A. Time histories and instantaneous spectra

The Zakharov equations were numerically integrated as described in the previous section using the parameter values of Table I (with the parameter $C$ allowed to vary). In order to study the dynamics of the driven waves, we look at the temporal evolution of the spatially averaged quantity $\langle|E|^2\rangle$, which is a global measure of the total energy in Langmuir waves. As the damping coefficient $C$ is varied, $\langle|E|^2\rangle$ is found to exhibit either periodic or apparently chaotic behavior (following an initial, transient phase). Figure 1 shows time histories of $\langle|E|^2\rangle$ for two specific values of the damping coefficient—the first ($C = 12.5$) exhibits a regular two cycle, whereas the second ($C = 6.25$) shows no simple periodicity and appears to be chaotic. In both cases, the observed dynamics of $\langle|E|^2\rangle$ in the many-mode Zakharov equations are found to be in agreement with that of the corresponding dynamics of the reduced three-mode system to be described in Secs. IV and V below.

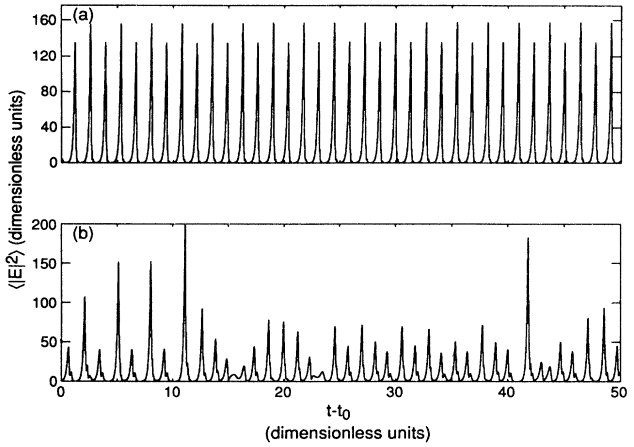


FIG. 1. Time histories of the spatially averaged $|E^2|$ from Zakharov-equation simulations using the parameters of Table I except for the Langmuir damping. (a) $\gamma = 12.5(k\lambda_e)^3\omega_e$ and (b) $\gamma = 6.25(k\lambda_e)^3\omega_e$.

Instantaneous Langmuir-wave and density wave number spectra are plotted in Fig. 2 at a *typical* time (in a sense that will be discussed shortly) for the parameters leading to the periodic behavior of Fig. 1(a). The Langmuir spectrum is localized in two regions of $k$ space as seen when $|E(k)|^2$ is plotted on a logarithmic scale in Fig. 2(a). The single unstable mode at $k\lambda_e = 0.04$ is $\sim 6$ orders of magnitude more intense than any of the surrounding modes. These neighboring modes, which result from the pairwise beating of daughter modes not exactly wave number matched to the pump (see Sec. III B), are energetically insignificant with regards to the mode-coupling dynamics. The second maximum in the Langmuir spectrum, which is in the vicinity of $k\lambda_e = -0.037$, corresponds to the daughter Langmuir waves in the backscatter decay of the beam mode. This component of the Langmuir spectrum is not concentrated in a single mode, but is distributed among a large number of modes as can be more clearly seen in Fig. 2(b), which is plotted on a linear scale, and which shows a magnified view of the wave numbers in the vicinity of the nominal backscattered Stokes wave number $k_S \equiv -k_b + k_*$.

The density spectrum $|\delta n(k)|^2$ at the same instant of time is plotted in Figs. 2(c) and 2(d). Because $\delta n(x)$ is a real quantity, its Fourier spectrum satisfies the symmetry condition $\delta n(k) = -\delta n^*(-k)$. We therefore can restrict consideration to those modes with $k > 0$. The dominant feature in the logarithmically scaled density spectrum of Fig. 2(c) is a peak in the vicinity of $k_{ia} = 2k_b - k_*$, as expected for the backscatter decay. There is also a component of the spectrum in the vicinity of $k = 0$ that results from the pairwise beating of backscattered Langmuir modes. This component is also energetically insignificant and will not be included in the reduction to a several-mode system in Sec. IV. The most intense density modes are plotted on a linear scale in Fig. 2(d). One can immediately see that there is a close correspondence between the shapes of the backscattered Langmuir spectrum in Fig. 2(b) and the density spectrum in Fig. 2(d) near their respective maxima. Specifically, the two are

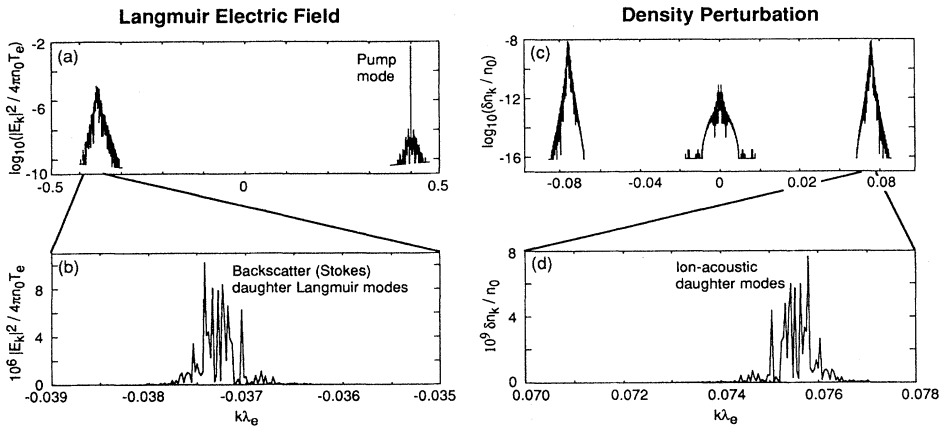


FIG. 2. Wave number spectra at a typical time during the simulation run corresponding to the time history of Fig. 1(a). (a) Langmuire spectrum $|E(k)|^2$ on a logarithmic scale showing both beam and backscatter modes. (b) Close-up of most intense backscatter modes on linear scale. (c) Density spectrum $|\delta n(k)|^2$ on logarithmic scale. (d) Close-up of most intense density modes on linear scale.

related (up to an overall amplitude scaling factor) by a reflection and translation in $k$ space:

$$|E_{k-k_S}|^2 \propto |\delta n_{k_{ia}-k}|^2. \tag{3}$$

Although the spectra of Fig. 2 are computed at a single, arbitrary time during the Zakharov-equation simulation, the spectral profiles at other times remain essentially unchanged. Only the relative intensities of the individual spectral components (i.e., the beam mode, the backscattered Langmuir modes, and the daughter density modes) are found to vary in time, with the relation described by Eq. (3) maintained. It is in this sense that we made our earlier claim that the spectra in Fig. 2 are typical. We now use this observed invariance of the spectral shape to construct a simple model for the time-dependent Langmuir and density spectra. It is this model that is the basis for our reduction of the multimode Zakharov-equation system to an equivalent three-mode system.

### B. Daughter-mode wave spectra: Shape functions and correlations

Motivated by relation (3) and the observation of an approximately time-independent shape, we express spectral amplitudes of the electric field and density perturbation in the following form:

$$E_k(t) \approx \tilde{E}(t)\xi_{k-k_S} e^{i\Phi(k-k_S,t)} + E_0(t)\delta_{k,k_b}, \tag{4a}$$

$$\delta n_k(t) \approx \widetilde{\delta n}(t)\xi^*_{k_{ia}-k} e^{i\Psi(k_{ia}-k,t)}. \tag{4b}$$

The respective arguments of the approximately time-independent *shape function* $\xi$ in (4a) and (4b) correspond to the arguments in (3), and are chosen so that $\xi_p$ is localized to the vicinity of $p = 0$. The second term on the right side of (4a) is the pump electric field, which is confined to a single mode at $k_b$, and which is assumed to be disjoint from the backscatter spectrum (i.e., $\xi_{k_b-k_S} = 0$).

The decomposition of $E_k(t) - E_0(t)\delta_{k,k_b}$ and $\delta n_k(t)$ into the product of $k$-independent amplitudes, time-independent shape functions $\xi$, and *phase* factors $\exp[i\Phi]$ and $\exp[i\Psi]$, which depend on both $k$ and $t$, is not unique. In particular, we allow each of $\tilde{E}$, $\widetilde{\delta n}$, and $\xi$ to be complex, even though they all could be stipulated as real quantities by absorbing the complex phases of $E$ and $\delta n$ entirely into $\Phi$ and $\Psi$. We choose this convention in order to facilitate the reduction to an equivalent three-wave system in Sec. IV. It is for this same reason that we express $\delta n$ in terms of $\xi^*$ instead of $\xi$.

Our numerical study shows that $\Phi$ and $\Psi$ develop negligibly small imaginary parts (hence, our reference to $\exp[i\Phi]$ and $\exp[i\Psi]$ as phase factors), provided that we require $\Phi$ and $\Psi$ to be strictly real at one particular time. For definiteness, the time corresponding to Fig. 2 will serve that purpose. Thus, only the magnitudes $|\tilde{E}\xi|$ and $|\widetilde{\delta n}\xi^*|$ can be inferred from Fig. 2. Full complex phase information is of course contained in the numerical Zakharov-equation solutions. It turns out, however, that sufficient phase information to allow a reduction to a three-wave system is contained in cross-correlation functions of $E$ and $\delta n$, as we now show. The following three correlation functions reflect different assumptions about the relative phase of $E$ and $\delta n$:

$$C(q) \equiv \left| \sum_{q_1,q_2=-q_{\max}}^{q_{\max}} E_{k_S+q_1}\delta n_{k_{ia}+q_2}\delta(q_1+q_2-q) \right|^2, \tag{5a}$$

$$C_{\max}(q) \equiv \left( \sum_{q_1,q_2=-q_{\max}}^{q_{\max}} |E_{k_S+q_1}\delta n_{k_{ia}+q_2}\delta(q_1+q_2-q)| \right)^2, \tag{5b}$$

$$C_{\mathrm{ran}}(q) \equiv \sum_{q_1,q_2=-q_{\max}}^{q_{\max}} |E_{k_S+q_1}\delta n_{k_{ia}+q_2}\delta(q_1+q_2-q)|^2. \tag{5c}$$

Sums rather than integrals are used in order to emphasize the discrete nature of the wave number spectra in the simulations. The limits on the sum $-q_{\max} \le q_i \le q_{\max}$ for $i = 1, 2$ are chosen to ensure that only modes in the vicinity of the nominal daughter-mode wave numbers contribute to the correlation functions.

The *true* correlation function $C(q)$ assumes the phases of $E_q$ and $\delta n_q$ to be those actually obtained from the numerical simulation. An upper bound on $C(q)$ is given by $C_{\max}(q)$, for which the phase of $E$ plus the phase of $\delta n$ is assumed to be independent of $k$. Finally, $C_{\rm ran}(q)$ employs a random-phase approximation and follows from (5a) upon assuming that the cross terms in the expansion of the square of the sum completely cancel (i.e., destructively interfere). To clarify the various assumptions about the phases, we substitute Eqs. (4) into Eqs. (5), where we note that the pump term in (4a) does not contribute:

$$C(q) = \left| \tilde{E}\widetilde{\delta n} \sum_{q_1, q_2 = -q_{\max}}^{q_{\max}} \xi_{q_1} \xi^*_{-q_2} \delta(q_1 + q_2 - q) e^{i[\Phi(q_1,t) + \Psi(-q_2,t)]} \right|^2, \tag{6a}$$

$$C_{\max}(q) = \left( |\tilde{E}\widetilde{\delta n}| \sum_{q_1, q_2 = -q_{\max}}^{q_{\max}} |\xi_{q_1} \xi^*_{-q_2} \delta(q_1 + q_2 - q)| \right)^2, \tag{6b}$$

$$C_{\rm ran}(q) = |\tilde{E}\widetilde{\delta n}|^2 \sum_{q_1, q_2 = -q_{\max}}^{q_{\max}} |\xi_{q_1} \xi^*_{-q_2} \delta(q_1 + q_2 - q)|^2. \tag{6c}$$

The correlation functions $C(q)$, $C_{\max}(q)$, and $C_{\rm ran}(q)$ were numerically computed from the Zakharov solutions (for the same value of $t$ as the spectra in Fig. 2), and are plotted on a logarithmic scale in Fig. 3 as a solid black curve, a solid gray curve, and a dashed black curve, respectively. Since $k_S + k_{ia} = k_b$, it follows that the variable $q$ is the mismatch between the beat wave number of the two daughter modes and the wave number of the beam-driven pump mode. (This mismatch should not be confused with the frequency mismatch to be discussed later—the vanishing of one does not imply the vanishing of the other.) At $q = 0$, which implies $q_1 = -q_2 \equiv p$, the true correlation function $C$ is very nearly equal to its upper bound $C_{\max}$, indicating that the product $E_{k_S+p} \delta n_{k_{ia}-p}$ as a function of $p$ exhibits maximal phase correlation. To show this, we set $q = 0$ in (6a) and (6b) yielding

$$C(0) = \left| \tilde{E}(t)\widetilde{\delta n}(t) \sum_{p=-q_{\max}}^{q_{\max}} |\xi_p|^2 e^{i[\Phi(p,t) + \Psi(p,t)]} \right|^2, \tag{7a}$$

$$C_{\max}(0) = \left( \tilde{E}(t)\widetilde{\delta n}(t) \sum_{p=-q_{\max}}^{q_{\max}} |\xi_p|^2 \right)^2. \tag{7b}$$

The near equality of $C(0)$ and $C_{\max}(0)$ would require $\Phi(p,t) + \Psi(p,t)$ to be approximately independent of $p$ if $\Phi$ and $\Psi$ were real phase angles. Although they are not strictly real, we can nevertheless draw the weaker conclusion

$$\frac{d}{dt} \sum_p |\xi_p|^2 e^{i[\Phi(p,t) + \Psi(p,t)]} \approx 0, \tag{8}$$

which will prove to be sufficient for our purposes.

The strong correlation between $E$ and $\delta n$ applies only to the case where the offset parameter $q$ vanishes. By contrast, for $q \neq 0$ Fig. 3 shows that $C(q) \ll C_{\rm ran}(q)$ indicating that phases of the products $E_{k_S+q_1} \delta n_{k_{ia}+q_2}$ are, on average, not merely *uncorrelated* when $q_2 \neq -q_1$, but are, in fact, strongly *anticorrelated*. It is this anticorrelation that accounts for the weakness of the Langmuir response in the modes surrounding the driven beam mode [Fig. 2(a)].

It is convenient to define $\xi$ so that it is normalized:

$$\sum_p |\xi_p|^2 = 1. \tag{9}$$

From (6a), (8), (9), and Fig. 3, it follows that

$$C(q,t) \approx |\tilde{E}(t)\widetilde{\delta n}(t)| \delta(q), \tag{10}$$

where the time dependence of $C(q)$ has been made explicit.

## IV. LUMPED-MODE REDUCTION OF ZAKHAROV EQUATIONS TO THREE-COUPLED-WAVE EQUATIONS

### A. Determination of reduced equations

Substitution of Eqs. (4) into (2) and separation of the driven and backscattered Langmuir components in (2a) yields

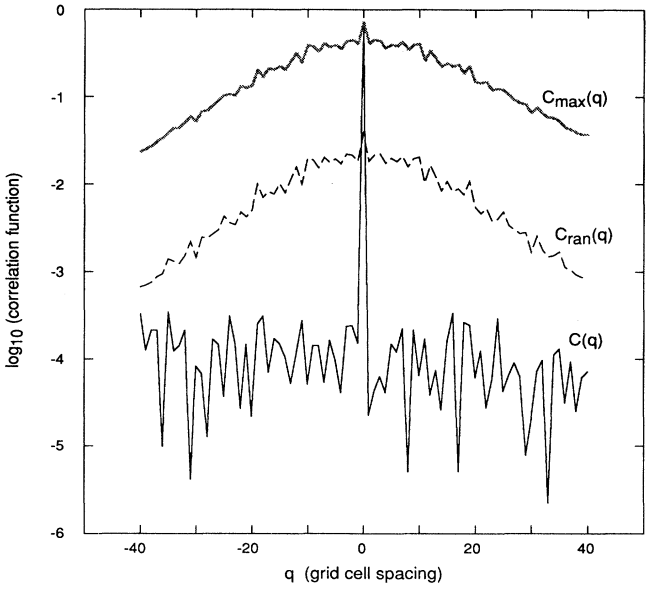


FIG. 3. Correlation functions (defined in text) $C(q)$ (solid black curve), $C_{\max}(q)$ (solid gray curve), and $C_{\rm ran}(q)$ (dashed black curve) on logarithmic scale vs wave number mismatch $q$.

$$[i\partial_t + i\gamma(k_b) - k_b^2]E_0 = \tilde{E}\widetilde{\delta n}\sum_p \xi^*_{k_{ia}-p}\xi_{k_b-p-k_S}e^{i[\Phi(k_b-p-k_S)+\Psi(k_{ia}-p)]}, \tag{11a}$$

$$[i\partial_t + i\gamma(k) - k^2]\tilde{E}\xi_{k-k_S}e^{i\Phi(k-k_S)} = E_0\widetilde{\delta n}^*\sum_p \xi_{p+k_{ia}}e^{-i\Psi(p+k_{ia})}\delta_{k-p,k_b}, \tag{11b}$$

$$[\partial_t^2 + 2\gamma_{ia}(k)\partial_t + k^2]\widetilde{\delta n}\xi^*_{k_{ia}-k}e^{i\Psi(k_{ia}-k)} = -k^2E_0\tilde{E}^*\sum_p \delta_{p,k_b}\xi^*_{p-k_S-k}e^{-i\Phi(p-k_S-k)}. \tag{11c}$$

The Fourier-transform symmetry relations $\delta n_{-k} = (\delta n_k)^*$ and $(E^*)_{-k} = (E_k)^*$ are used on the right sides of (11b) and (11c), respectively. The summations in Eqs. (11) can be explicitly evaluated resulting in the coupled system

$$[i\partial_t + i\gamma(k_b) - k_b^2]E_0(t) = \tilde{E}(t)\widetilde{\delta n}(t), \tag{12a}$$

$$[i\partial_t + i\gamma(k) - k^2]\tilde{E}(t)e^{i\Phi(k-k_S,t)}\xi_{k-k_S} = E_0(t)\widetilde{\delta n}^*(t)\xi_{k-k_S}e^{-i\Psi(k-k_S,t)}, \tag{12b}$$

$$[\partial_t^2 + 2\gamma_{ia}(k)\partial_t + k^2]\widetilde{\delta n}(t)\xi^*_{ia-k}e^{i\Psi(k_{ia}-k,t)} = -k^2E_0(t)\tilde{E}^*(t)\xi^*_{k_{ia}-k}e^{-i\Phi(k_{ia}-k,t)}. \tag{12c}$$

The (near) equality of (7a) and (7b) has been used, together with Eq. (8) and the identity $k_S + k_{ia} = k_b$. Note that each of Eqs. (12b) and (12c) actually represents a multiplicity of equations (as many as there are values of $p$ for which $\xi_p$ does not vanish).

We can, nevertheless, reduce (12b) and (12c) to two single equations describing the evolution of *equivalent lumped modes.* Multiplying (12b) by $\xi^*_{k-k_S}\exp[i\Psi(k-k_S,t)]$ and summing over $k$ yields

$$\sum_k |\xi_{k-k_S}|^2e^{i[\Phi+\Psi]}[i\partial_t + i\gamma(k) - k^2 - \dot{\Phi}]\tilde{E}(t) = E_0(t)\widetilde{\delta n}^*, \tag{13a}$$

where the term $\dot{\Phi}$ results from passing the operator $\partial_t$ to the right of $\exp[i\Phi]$. Similarly, multiplying (12c) by $\xi_{k_{ia}-k}\exp[i\Phi(k_{ia}-k,t)]$ yields

$$\sum_k |\xi_{k_{ia}-k}|^2e^{i[\Phi+\Psi]}[\partial_t^2 + 2\gamma_{ia}(k)\partial_t + k^2 + i\ddot{\Psi} - \dot{\Psi}^2 + 2i\gamma_{ia}\dot{\Psi}]\widetilde{\delta n}(t) = E_0(t)\tilde{E}^*. \tag{13b}$$

The explicit dependencies of $\Phi$ and $\Psi$ have been left out of Eqs. (13) for compactness.

We make the *ansatz* (to be defended shortly) that Eqs. (13a) and (13b) are equivalent to single-mode equations of the form

$$(i\partial_t + i\bar{\gamma}_S - \bar{k}_S^2)\tilde{E}(t) = E_0(t)\widetilde{\delta n}^*(t), \tag{14a}$$

and

$$(\partial_t^2 + 2\bar{\gamma}_{ia}\partial_t + \bar{k}_{ia}^2)\widetilde{\delta n}(t) = -\bar{k}_{ia}^2E_0(t)\tilde{E}^*(t), \tag{14b}$$

where $\bar{k}_S$, $\bar{\gamma}_S$, $\bar{k}_{ia}$, and $\bar{\gamma}_{ia}$ are the effective wave number and damping rate of the equivalent lumped (Stokes) Langmuir and ion-acoustic modes. Multiplying (14a) by $|\xi(k-k_S)|^2\exp i[\Phi(k-k_S)+\Psi(k-k_S)]$ and summing over $k$ yields

$$\sum_k |\xi_{k-k_S}|^2e^{i[\Phi(k-k_S,t)+\Psi(k-k_S,t)]}(i\partial_t + i\bar{\gamma}_S - \bar{k}_S^2)\tilde{E}(t) = E_0(t)\widetilde{\delta n}^*(t). \tag{15}$$

A sufficient condition for the equivalence of (13a) and (15) is a term-by-term correspondence which implies

$$\{\dot{\Phi}(k-k_S,t) - i[\gamma(k) - \bar{\gamma}_S] + (k^2 - \bar{k}_S^2)\}\tilde{E}(t) = 0, \tag{16}$$

at those modes for which $\xi(k-k_S)$ does not vanish. It is clear that if $\gamma(k)$ is not everywhere equal to $\bar{\gamma}_S$, then $\Phi$ will indeed develop an imaginary part as discussed earlier. Equation (16) predicts $\dot{\Phi}$ is complex and independent of $t$, which would result in the monotonic increase or decrease of $|\exp[i\Phi(t)]|$ (depending on the sign of the imaginary part of $\dot{\Phi}$). Such a secular change in magnitude is inconsistent with the observation that $|\xi\exp[i\Phi]|$ is approximately constant with time. However, during the nonlinear evolution of the PDE system $\tilde{E}(t)$ periodically approaches zero. It is at these times that $\dot{\Phi}$ is not constrained to satisfy the vanishing of the factor inside the curly brackets in (16). One possible way to avoid such secular growth—inconsistent with observation—would be for the imaginary part of $\Phi$ to be reset to zero at these times. Thus $\Phi$ would never develop a sufficient imaginary part for $|\exp[i\Phi]|$ to differ significantly from unity.

In order to determine the lumped-mode parameters $\bar{\gamma}_S$ and $\bar{k}_S$, we use Eq. (8), which implies

$$\sum_k [\dot{\Phi}(k-k_S) + \dot{\Psi}(k-k_S)]e^{i[\Phi+\Psi]}|\xi_{k-k_S}|^2 = 0. \tag{17a}$$

If we make the stronger assumption that

$$\sum_k \dot{\Phi}(k-k_S)e^{i[\Phi+\Psi]}|\xi_{k-k_S}|^2 = 0,$$
$$\sum_k \dot{\Psi}(k-k_S)e^{i[\Phi+\Psi]}|\xi_{k-k_S}|^2 = 0, \tag{17b}$$

hold independently, it immediately follows from (16) that

$$\bar{\gamma}_S = \sum_k \gamma(k)|\xi_{k-k_S}|^2 \tag{18a}$$

and

$$\bar{k}_S = \left(\sum_k k^2|\xi_{k-k_S}|^2\right)^{1/2}. \tag{18b}$$

Here we make the evaluation at the particular time (i.e., the time corresponding to Fig. 2) when $\exp(i[\Phi+\Psi]) = 1$ is imposed for all $k$. Although conditions allowing one to infer (17b) from (17a) do not necessarily follow from the observed spectral correlations, this step nevertheless leads to parameters of the reduced lumped-mode system that accurately reproduce the dynamics of the multimode Zakharov-equation system (see Sec. V A).

Following a similar procedure for the system of second-order density equations (13b) yields an equation analogous to (16), but for the time derivatives of $\Psi$

$$[i\ddot{\Psi} - \dot{\Psi}^2 + 2i\gamma_{ia}\dot{\Psi} + 2(\gamma_{ia}-\bar{\gamma}_{ia})\partial_t + k^2 - \bar{k}_{ia}^2]\widetilde{\delta n}(t) = 0. \tag{19}$$

We can replace $\partial_t\widetilde{\delta n}$ by $\bar{\omega}_{ia}\widetilde{\delta n}$ where $\bar{\omega}_{ia}$ is independent of $k$ and is near the resonant ion-acoustic frequency at $k = k_{ia}$. The frequency $\bar{\omega}_{ia}$ will, nevertheless, depend on time; however, we will assume that this time dependence is sufficiently small to allow us to drop the term proportional to $\ddot{\Psi}$ in (19). We will also drop the $\dot{\Psi}^2$ from (19) on the assumption that variations in $\gamma_{ia}$ and $k_{ia}$ are small relative to their typical values (e.g., $\bar{\gamma}_{ia}$ and $\bar{k}_{ia}$ as defined below). This condition is indeed met for the spectra under consideration here.

Upon making the above approximations we arrive at the following expressions for the ion-acoustic lumped-mode parameters:

$$\bar{\gamma}_{ia} = \left(\sum_k [1/\gamma_{ia}(k)]|\xi_{k_{ia}-k}|^2\right)^{-1}, \tag{20a}$$

and

$$\bar{k}_{ia} = \left(\bar{\gamma}_{ia}\sum_k [k^2/\gamma_{ia}]|\xi_{k_{ia}-k}|^2\right)^{1/2}. \tag{20b}$$

### B. Transformation to a standard form

Equations (12a), (14a), and (14b) together constitute a system of three coupled ordinary differential equations in three complex variables. Because Eq. (14b) is second order, there are a total of eight degrees of freedom in this system. We will, however, later approximate (14b) by a first-order system in order to make contact with the previously studied system of WFO, which they showed to have only four *independent* degrees of freedom (see Sec. VI below). These equations simplify upon making the change of variables $(E_0, \tilde{E}, \widetilde{\delta n}) \to (A_1, A_2, A_3)$, where

$$E_0 = \left(\frac{2}{\bar{k}_{ia}}\right)^{1/2} A_1 e^{-ik_b^2 t}, \tag{21a}$$
$$\tilde{E} = \left(\frac{2}{\bar{k}_{ia}}\right)^{1/2} A_2 e^{-i\bar{k}_S^2 t}, \tag{21b}$$
$$\widetilde{\delta n} = iA_3 e^{-i\bar{k}_{ia}t}. \tag{21c}$$

This change of variables expresses the field variables in terms of a (slowly varying) amplitude modulating the characteristic linear wave frequency. Note that in the case of the Langmuir waves this represents a *second envelope approximation* since the field $E$ in (1) is already an envelope field modulating fast oscillations at the electron plasma frequency $\omega_e$.

Substituting Eqs. (21) into (12a), (14a), and (14b) yields the system

$$(\partial_t + \gamma_b)A_1(t) = A_2A_3e^{i\delta\omega t}, \tag{22a}$$
$$(\partial_t + \bar{\gamma}_S)A_2(t) = -A_1A_3^*e^{-i\delta\omega t}, \tag{22b}$$
$$\left(\frac{i}{2\bar{k}_{ia}}\partial_t^2 + \left[1 + i\frac{\bar{\gamma}_{ia}}{\bar{k}_{ia}}\right]\partial_t + \bar{\gamma}_{ia}\right)A_3 = -A_1A_2^*e^{-i\delta\omega t}. \tag{22c}$$

The linear frequency mismatch is

$$\delta\omega = k_b^2 - \bar{k}_S^2 - \bar{k}_{ia},$$

and would vanish for a resonant backscatter decay (i.e., $\bar{k}_S = k_S$ and $\bar{k}_{ia} = k_{ia}$). We have also employed the simplified notation $\gamma_b \equiv \gamma(k_b)$.

### C. Further reduction in degree of system

If the amplitude $A_3$ varies sufficiently slowly relative to the linear ion-acoustic frequency (i.e., $|\partial_t A_3| \ll |\bar{k}_{ia}A_3|$) and the ion-acoustic mode is weakly damped ($|\bar{\gamma}_{ia}| \ll |\bar{k}_{ia}|$), then Eq. (22c) reduces to

$$(\partial_t + \bar{\gamma}_{ia})A_3 = -A_1A_2^*e^{-i\delta\omega t}. \tag{23}$$

We note that in this limit the approximations following (19) become exact. Equations (22a), (22b), and (23) are equivalent to the three-mode system studied in WFO (prior to imposing the condition $\bar{\gamma}_S = \bar{\gamma}_{ia}$). In comparing the Zakharov-equation dynamics of Sec. III with the dynamics of the coupled three-mode system, we will use both (22c) and (23).

## V. COMPARISON OF ZAKHAROV-EQUATION AND REDUCED LUMPED-MODE DYNAMICS

The equivalent-lumped-mode parameters of Eqs. (18) and (20) were numerically computed for the two Zakharov-equation simulations of Fig. 1 using the $k$-space spectra of Fig. 2 and corresponding ones (not shown) for the chaotic case of Fig. 1(b). These parameter values are listed in Table II. Note that in these units the pump wave number is $k_b = 10.28$. The wave numbers $\bar{k}_S$ and $\bar{k}_{ia}$ are sufficiently different for the two cases to result in a change of sign in the effective frequency mismatch $\delta\omega$. These values of $\delta\omega$ are small, but not negligible—especially in the first case where $\delta\omega$ is approximately 50% of the ion-acoustic damping rate.

### A. Dynamics with second-order density response

Because the lumped-mode parameters of Table II are determined from Zakharov-equation simulations, which employ a second-order density response, Eq. (22c) will more accurately describe the density response in the truncated model than will Eq. (23). We therefore consider solutions to the fourth-order complex system (22a)–(22c) first.

Time histories of $|E_0|^2 + |\tilde{E}|^2 = 2(|A_1|^2 + |A_2|^2)/\bar{k}_{ia}$ are plotted in Fig. 4 for a time interval equal to that in Fig. 1. This quantity equals the spatially averaged squared Langmuir field in the three-mode system and thus can be compared directly with $\langle |E|^2 \rangle$ in Fig. 1. In these runs, the second-order equation (22c) for the density response is used. For the first (two-cycle) case, the time histories in Figs. 1(a) and 4(a) are quite similar [following an initial transient in Fig. 4(a)] with nearly the same periodicity and amplitude. The relative difference in amplitude of the alternating high and low peaks is, however, somewhat larger for the three-mode approximation. The chaotic dynamics in Figs. 1(b) and 4(b) are also comparable although it is more difficult to make a quantitative comparison for the relatively short time intervals shown.

The level of agreement found between the lumped-mode dynamics and the corresponding multimode Zakharov-equation dynamics supports the truncation procedure of the previous sections.

### B. Dynamics with first-order density response

If Eq. (22c) is replaced by Eq. (23), the dynamics are found to change, with poorer agreement between the Zakharov-equation and lumped-mode solutions using the (nominal) parameters of Table II. Figure 5 shows time histories of $|E_0|^2 + |\tilde{E}|^2$ for the system of three complex first-order equations using the parameters of the first row of Table II except for the value $\delta\omega/|\gamma_b|$, which is set to the value in the table (0.40), twice the value in the table (0.80) and three times the value in the table (1.20), and plotted in Figs. 5(a), 5(b), and 5(c), respectively. In Fig. 5(a) [i.e., the same parameters as for Fig. 4(a)], the two-cycle behavior is lost and the dynamics appears to be chaotic, suggesting a qualitative change in the dynamics. Doubling the frequency mismatch [Fig. 5(b)] recovers the two-cycle behavior but the period is somewhat shorter and the maximum amplitude is smaller than in Fig. 4(a). A further 50% increase in $\delta\omega$ [Fig. 5(c)] results in a simple limit cycle with still shorter period and smaller maximum amplitude. Thus, we find that the qualitative behavior of the system is maintained, despite the reduction of the degree of the system, provided suitable adjustments in the parameters of the lumped-mode system (e.g., $\delta\omega$) are made. The approximate validity of the third-order system follows from the relatively weak ion-acoustic damping ratio in the Zakharov-equation simulations (i.e., $\gamma_{ia} = 0.2kc_s$ from Table I). We will restrict consideration to the system of three complex first-order equations in the following sections.

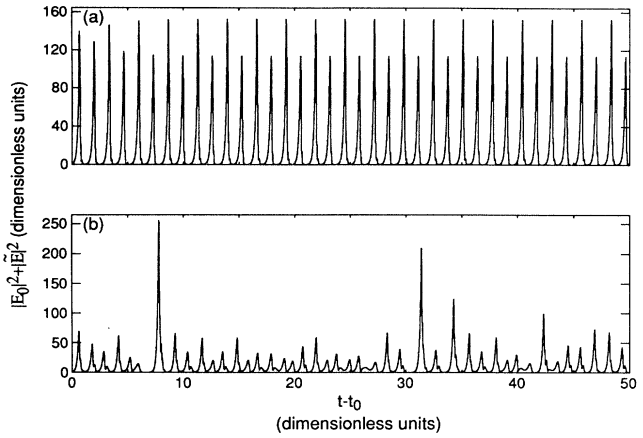


FIG. 4. Time histories of $E_0^2 + \tilde{E}^2$ for the three-mode system with second-order density response of Eqs. (17). (a) Parameters from first row of Table II. (b) Parameters from the second row of Table II.

## VI. ANALYTICAL DISCUSSION OF THREE-WAVE MODEL

We have shown numerically that under certain conditions the physical system described by the Zakharov PDE's reduces to three simple wave equations with com-

TABLE II. Effective lumped-mode parameters.

| Regime | $\gamma(k \neq k_b)$ | $\bar{k}_S$ | $\bar{\gamma}_S/\lvert\gamma_b\rvert$ | $\bar{k}_{ia}$ | $\bar{\gamma}_{ia}/\lvert\gamma_b\rvert$ | $\delta\omega/\lvert\gamma_b\rvert$ |
|---|---|---|---|---|---|---|
| Regular | $12.5(k\lambda_e)^3\omega_e$ | 9.19 | 5.71 | 19.48 | 0.88 | 0.40 |
| Chaotic | $6.25(k\lambda_e)^3\omega_e$ | 9.32 | 2.98 | 19.60 | 0.89 | −0.15 |

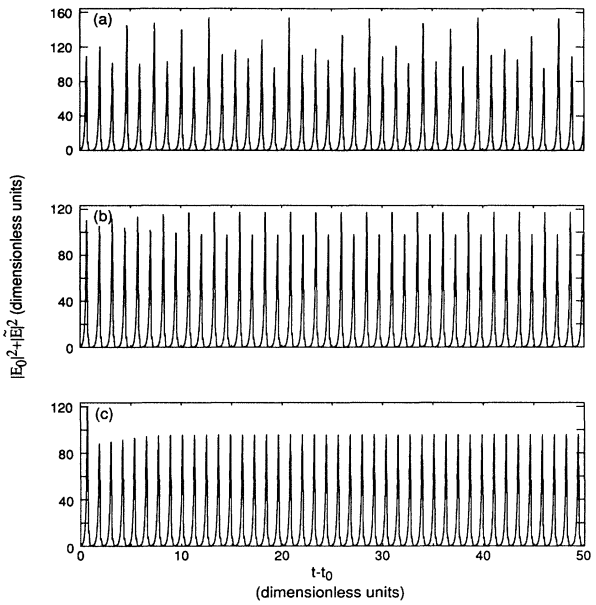


FIG. 5. Time histories of $E_0^2 + \tilde{E}^2$ for the three-mode system with first-order density response of Eqs. (17a), (17b), and (18). (a) Parameters from first row of Table II. (b) Same as (a) except that $\delta\omega/|\gamma_b| = 0.80$. (c) Same as (a) except that $\delta\omega/|\gamma_b| = 1.20$.

plex amplitudes. We now examine the analytical stability of these equations.

### A. Reduction to a *real* four-dimensional system

We begin by rewriting the equations in the same form as used by WFO so that we can directly compare our analysis to theirs. Upon making the change of variables,

$$t = \frac{-\tilde{t}}{\gamma_b}, \quad \delta\omega = \Delta\gamma_b, \quad \bar{\gamma}_s = -\gamma_b\Gamma_2, \quad \bar{\gamma}_{ia} = -\gamma_b\Gamma_3,$$
$$A_i = -\gamma_b\tilde{A}_i, \quad i = 1,2,3,$$

in Eqs. (22a), (22b), and (23), we recover the following system, which is equivalent to WFO's Eqs. (2a) and (2b):

$$\frac{d}{dt}\tilde{A}_1 = \tilde{A}_1 + [\tilde{A}_2\tilde{A}_3]e^{-i\tilde{t}\Delta}, \tag{24a}$$
$$\frac{d}{dt}\tilde{A}_2 = -\Gamma_2\tilde{A}_2 - [\tilde{A}_1\tilde{A}_3^*]e^{i\tilde{t}\Delta}, \tag{24b}$$
$$\frac{d}{dt}\tilde{A}_3 = -\Gamma_3\tilde{A}_3 - [\tilde{A}_1\tilde{A}_2^*]e^{i\tilde{t}\Delta}. \tag{24c}$$

At this point in their analysis, WFO express $\tilde{A}_1$, $\tilde{A}_2$, and $\tilde{A}_3$ in terms of moduli and phases, i.e.,

$$\tilde{A}_1 = a_1e^{i\phi_1}, \tag{25a}$$
$$\tilde{A}_2 = a_2e^{i[\phi_2+\tilde{t}\Delta/2]}, \tag{25b}$$
$$\tilde{A}_3 = a_3e^{i[\phi_3+\tilde{t}\Delta/2]}, \tag{25c}$$
$$\phi = \phi_1 - \phi_2 - \phi_3, \tag{25d}$$

thereby reducing the equations to a fourth-order real system

$$\frac{d}{dt}a_1 = a_1 + a_2a_3\cos\phi, \tag{26a}$$
$$\frac{d}{dt}a_2 = -\Gamma_2a_2 - a_1a_3\cos\phi, \tag{26b}$$
$$\frac{d}{dt}a_3 = -\Gamma_3a_3 - a_1a_2\cos\phi, \tag{26c}$$
$$\frac{d}{dt}\phi = -\Delta + \frac{a_1^2a_2^2 + a_1^2a_3^2 - a_2^2a_3^2}{a_1a_2a_3}\sin\phi, \tag{26d}$$

where we have made the substitution $\tilde{t} \to t$ for the sake of simplicity.

WFO show that in the special case $\Gamma_2 = \Gamma_3 = \Gamma$, the quantity $a_2^2 - a_3^2$ decreases exponentially. They therefore set $a_2 = a_3$ and use the resulting real third-order system without loss of information. Their entire analysis is limited to this case. However, in our circumstance $a_2$ and $a_3$ represent two different waves, Langmuir and ion acoustic, so there is no physical reason why we should assume that the damping rates are equal. We thus retain the more general fourth-order real system (26).

### B. Stability analysis

The stability analysis undertaken in this section is similar to that of WFO, but modified for the four-dimensional system.

#### *1. Fixed point stability*

We first look at the local stability of the steady state solution, i.e., the fixed point. A stationary solution to Eqs. (26) is

$$a_{1,0} = -\frac{\sqrt{\Gamma_2\Gamma_3}}{\cos\phi_0}, \tag{27a}$$
$$a_{2,0} = \frac{\sqrt{\Gamma_3}}{\cos\phi_0}, \tag{27b}$$
$$a_{3,0} = \frac{\sqrt{\Gamma_2}}{\cos\phi_0}, \tag{27c}$$
$$\phi_0 = \tan^{-1}\left[\frac{\Delta}{1-\Gamma_3-\Gamma_2}\right]. \tag{27d}$$

There is also a trivial solution $a_{1,0} = a_{2,0} = a_{3,0} = 0$, but this is always unstable since $a_1$ is linearly unstable.

We linearize Eqs. (26) for perturbations about the 4D fixed point solution $a_j = a_{j,0} + \epsilon_j$; $j = 0,1,2,3$ (where $a_{0,0} = \phi_0$). The perturbations vary as $\epsilon_j = \epsilon_{j,0}e^{\lambda t}$. The resulting eigenvalue equation is quartic in $\lambda$. We use Hurwitz's criterion [22] to determine the bounding surface of the stable region of parameter space for which $\mathrm{Re}(\lambda) \le 0$ for all eigenvalues $\lambda$. Figure 6 shows contours of the marginal value of $\Delta$ plotted in $\Gamma_2 - \Gamma_3$ space, where the fixed point is locally stable if $\Delta$ exceeds this marginal value.

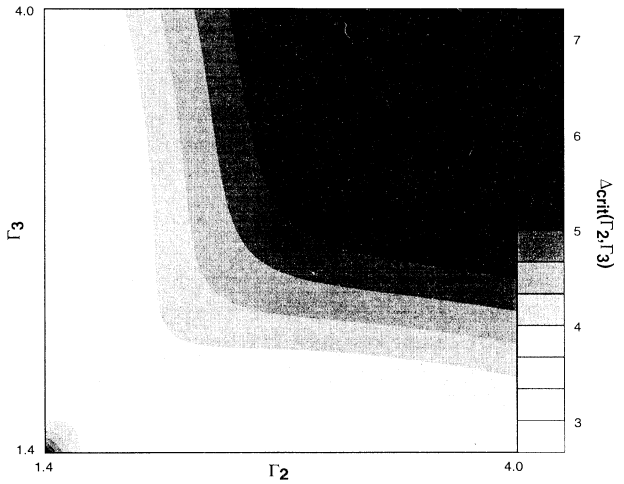


FIG. 6. Contours showing the lower bound on the value of $\Delta$ for local fixed point stability in $\Gamma_2$–$\Gamma_3$ space. Values along the diagonal ($\Gamma_2 = \Gamma_3$) correspond to Fig. 1 of WFO.

### 2. *Four-volume contraction*

One necessary condition for stable orbits in a dissipative system is that phase-space volumes (or the four-dimensional equivalent) contract. The rate of divergence of phase-space flow for our system can be shown to be $2 - \Gamma_2 - \Gamma_3$. Therefore four-volume in phase space varies in time according to $V(t) = V(0)\exp[(2 - \Gamma_2 - \Gamma_3)t]$, so that for $\Gamma_2 + \Gamma_3 > 2$, four-volumes shrink exponentially. This is a generalization of WFO's similar constraint that $\Gamma > 1$. Here, $\Gamma_2 + \Gamma_3 < 2$ implies unbounded orbits because the damping rates of the daughter waves are too low to saturate the instability of the pump wave.

### 3. *Frequency mismatch*

In WFO's three-dimensional case, $\Delta = 0$ leads to divergent orbits in all cases. However, different damping rates for the two daughter waves allow nonlinearly stabilized dynamic solutions to exist for $\Delta = 0$. This is a physically interesting case because the fastest linear growth rate in a three-wave parametric instability occurs at $\Delta = 0$.

When $\Delta = 0$, our real fourth-order set of equations contracts into a third-order system different from that of WFO. In order to demonstrate this, we sum Eqs. (26a)–(26c) after multiplying by $a_2a_3$, $a_1a_3$, and $a_1a_2$, respectively, and set $\Delta = 0$ in (26d), yielding

$$\frac{d}{dt}(a_1a_2a_3) = a_1a_2a_3(1 - \Gamma_2 - \Gamma_3) - (a_1^2a_2^2 + a_1^2a_3^2 - a_2^2a_3^2)\cos\phi, \tag{28a}$$

$$\frac{d\phi}{dt} = \frac{a_1^2a_2^2 + a_1^2a_3^2 - a_2^2a_3^2}{a_1a_2a_3}\sin\phi. \tag{28b}$$

Combining these equations leads to

$$\frac{d\phi}{dt} = -\left(\frac{1}{a_1a_2a_3}\frac{d}{dt}[a_1a_2a_3] + [\Gamma_3 + \Gamma_2 - 1]\right)\tan\phi, \tag{28c}$$

which reduces to

$$\frac{d}{dt}[\ln(a_1a_2a_3\sin\phi)] = -(\Gamma_3 + \Gamma_2 - 1). \tag{28d}$$

The quantity $\Gamma_3 + \Gamma_2 - 1$ is always positive in the domain of bounded solutions; therefore, the product $a_1a_2a_3\sin\phi$ decays to zero exponentially with time, reducing the order of the system from four to three. The contraction from four to three dimensions can be seen in Fig. 7, which show the early-time numerical solutions of Eqs. (24) for the case $\Gamma_2 = 2.0, \Gamma_3 = 1.8$, and $\Delta = 0$. The three amplitudes in Figs. 7(a)–7(c) will eventually settle into a limit cycle. Figure 7(d) shows that the phase $\phi$ defined by (24c), which is given an initial value of $\pi/2$, becomes more and more localized to the vicinity of, alternately, 0 and $\pi$. Finally, the product $a_1a_2a_3\sin\phi$ is seen in Fig. 7(e) to decay exponentially, as predicted by (28d), until numerical limits imposed by roundoff error are exceeded—more than 20 $e$-foldings below the initial

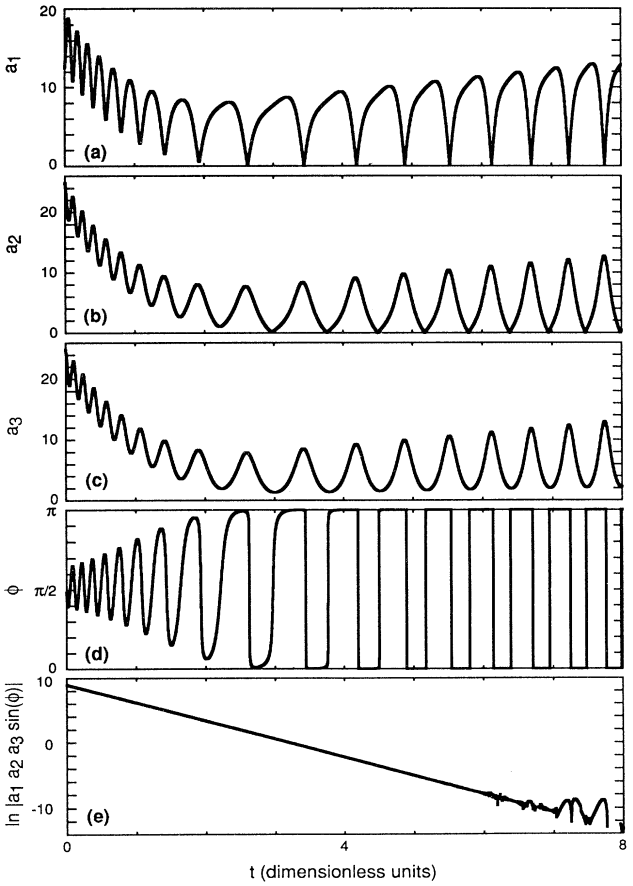


FIG. 7. Numerical solutions to Eqs. (24) for parameters $\Gamma_2 = 2.0$, $\Gamma_3 = 1.8$, and $\Delta = 0$. (a) $a_1$ vs $t$, (b) $a_2$ vs $t$, (c) $a_3$ vs $t$, (d) $\phi$ vs $t$, and (e) $\ln[a_1a_2a_3\sin\phi]$ vs $t$.

value. From Fig. 7 we see that when $a_1$ or $a_2$ vanishes, $\phi$ jumps between 0 and $\pi$.

In the limit $t \to \infty$, the value of $\cos\phi$ will alternate between $+1$ and $-1$, with the sign change occurring simultaneously with the vanishing of one of the $a_i$. Thus, Eqs. (26a)–(26c) become

$$\frac{d}{dt}a_1 = a_1 \pm a_2 a_3, \tag{29a}$$

$$\frac{d}{dt}a_2 = -\Gamma_2 a_2 \mp a_1 a_3, \tag{29b}$$

$$\frac{d}{dt}a_3 = -\Gamma_3 a_3 \mp a_1 a_2. \tag{29c}$$

Note that when, for example, $a_1$ vanishes, $\dot{a}_1$ changes sign while $\dot{a}_2$ and $\dot{a}_3$ remain unchanged.

Equations (29) are equivalent to a three-dimensional system of equations, in which the *real* variables $b_i$ can be either positive or negative,

$$\frac{d}{dt}b_1 = b_1 + b_2 b_3, \tag{30a}$$

$$\frac{d}{dt}b_2 = -\Gamma_2 b_2 - b_1 b_3, \tag{30b}$$

$$\frac{d}{dt}b_3 = -\Gamma_3 b_3 - b_1 b_2. \tag{30c}$$

The *amplitudes* $a_j$ in (29) are related to the variables $b_j$ through the relation $a_j = |b_j|$; $j = 1, 3$.

## VII. NUMERICAL ANALYSIS OF THREE-WAVE MODEL

We use a Runge-Kutta integrating routine to numerically evolve the system of Eqs. (26). We see repeated dips into and out of chaos as limit cycles appear via tangent bifurcations and then cascade back into chaos, usually by way of a period doubling bifurcation.

We look at a range of values of the growth and damping rates encompassing those used in the numerical evolution of the complete Zakharov equations discussed above (see Table II). Damping rates $\Gamma_2$ and $\Gamma_3$ are sampled from the range $1 \le \Gamma_{2,3} \le 20$ for both the case of $\Delta = 2$ and $\Delta = 0$. The value $\Delta = 2$ is chosen because it is the one studied by WFO.

Since a full two-dimensional scan of $\Gamma_2$ and $\Gamma_3$ is computationally prohibitive, we focus on four cases: $\Delta = 0$, with $\Gamma_2 = 2.5$ and 9, and $\Delta = 2$, with $\Gamma_2 = 2.5$ and 9. The parameter $\Gamma_3$ is varied between 0 and 20 by steps of 0.1. The time series solution for $a_1$ is followed through approximately 30 cycles for each value of $\Gamma_3$ to determine whether there is a stable limit cycle or chaos. Figure 8 shows examples of both chaos and a limit cycle, as evidenced by orbits in $a_1 - a_2 - a_3$ space and by time series of $a_1$ vs $t$.

Figure 9 shows a summary of the observed behavior. The dark bands represent chaotic solutions, the white bands represent limit cycles of finite order. Figure 9(a) shows results for the case $\Delta = 0$, with $\Gamma_2 = 2.5$. Note the dashed line at $\Gamma_3 = 2.5$. Here $\Gamma_2 = \Gamma_3$ and the system reduces to WFO's three-dimensional system where all orbits with $\Delta = 0$ diverge. Indeed, both the amplitude and frequency of the stable limit cycle right below $\Gamma_3 = 2.5$ increase as $\Gamma_2 \to \Gamma_3$ until at $\Gamma_3 = 2.5$ they diverge. Just above $\Gamma_3 = 2.5$, the stable limit cycle reappears with decreasing amplitude and frequency until at $\Gamma_3 = 3.6$ a period doubling cascade occurs, followed by a transition into chaos. Figure 9(b) shows the case $\Delta = 0$, with $\Gamma_2 = 9$. This solution also diverges at $\Gamma_3 = \Gamma_2 = 9$. In the two $\Delta = 2$ cases the behavior at $\Gamma_2 = \Gamma_3$ corresponds exactly to the behavior observed by WFO. Figure 9(c) shows a dot-dashed line at $\Gamma_2 = \Gamma_3 = 2.5$; here the system is oscillatory with an envelope that grows rapidly. The instability has not yet saturated. Interestingly, just below and above this critical value of $\Gamma_3$ there is a stable limit cycle that loses stability right at $\Gamma_3 = 2.5$. Figure 5(b) also has a dotted line at $\Gamma_3 = 1$; below this value of $\Gamma_3$ the fixed point is stable. When $\Delta = 2, \Gamma_2 = \Gamma_3 = 9$, as shown in Fig. 9(d), there is just a simple two-cycle as is observed by WFO.

The "observational" method of looking at time series and orbits is a fairly accurate way of determining parameters for which the system is chaotic or stable, but it is not conclusive. To rigorously analyze order vs chaos one needs to determine Lyapunov numbers, which represent

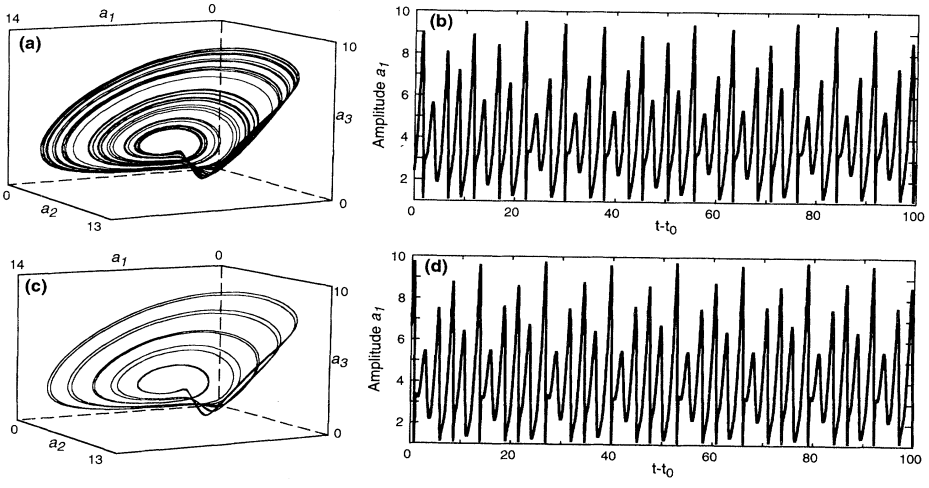


FIG. 8. "Observational" evidence of chaotic and limit-cycle behavior: (a) shows a chaotic orbit for the amplitudes $a_1(t)$, $a_2(t)$, and $a_3(t)$ with the parameters $\Delta = 2$, $\Gamma_2 = 2.5$, and $\Gamma_3 = 6.0$. (b) shows the time series $a_1(t)$ for the same parameters. (c) and (d) show the orbit and time series for a nearby set of parameters ($\Delta = 2$, $\Gamma_2 = 2.5$, and $\Gamma_3 = 6.0$) exhibiting a periodic ten-cycle.

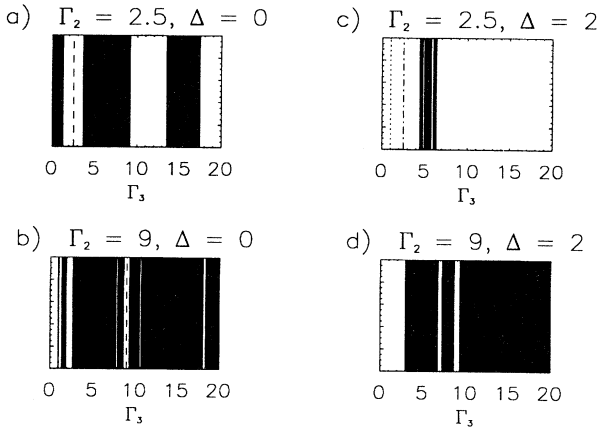


FIG. 9. Qualitative description of chaos and order. The black bands represent chaos and the white ones periodic behavior. Four regimes are examined: (a) $\Gamma_2 = 2.5$, $\Delta = 0$ (the dashed line represents diverging orbits); (b) $\Gamma_2 = 9, \Delta = 0$ (the dashed line represents diverging orbits); (c) $\Gamma_2 = 2.5, \Delta = 2$ (below the dotted line the fixed point is stable, again the dashed line represents diverging orbits); and (d) $\Gamma_2 = 9, \Delta = 2$.

the rate at which nearby orbits exponentially diverge. There are four Lyapunov numbers for our system, one for each degree of freedom. We need only consider the largest value. A largest Lyapunov number less than zero would imply a stable fixed point, one equal to zero would mean a stable limit cycle, and one greater than zero implies chaos.

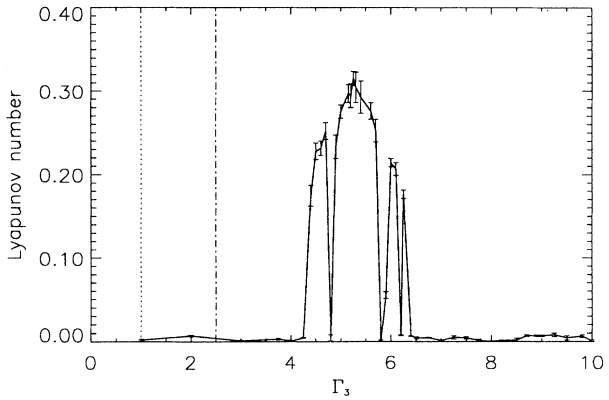


FIG. 10. A detailed analysis using Lyapunov numbers (arbitrary units) of the $\Gamma_2 = 2.5, \Delta = 2$ case. For $\Gamma_3 < 1$ (below the dotted line) the fixed point is stable. At $\Gamma_3 = 2.5$, the orbits diverge as the system contracts onto the three-dimensional system of WFO. Tangent bifurcations are seen at $\Gamma_3 = 4.8$, 5.8, 6.2, and 6.4. As the calculation is particularly sensitive to variation in two of the input parameters to the Lyapunov code, they were allowed to vary and the error bars represent the associated change in the Lyapunov number. Specifically, the maximum displacement allowed between evolving orbits is varied from 10 to 15% of the range of time series values, and the length of an evolving step is varied between $\frac{1}{3}$ and $\frac{1}{4}$ of the period of oscillation in the time series.

We have employed a computer code [23] that estimates the largest Lyapunov number for a given time series, based on the method of time delay reconstruction. We have used this analysis for the $\Delta = 2$, with $\Gamma_2 = 2.5$ case seen in Fig. 9(c), extending the time series to approximately 300 cycles. Figure 10 shows the results. The regions of order and chaos are seen clearly. For $\Gamma_3 < 1$, the fixed point is stable. At $\Gamma_3 = 1$, a limit cycle emerges via a Hopf bifurcation. At $\Gamma_3 = 2.5$, as noted above, the amplitude of the limit cycle diverges. At $\Gamma_3 = 4$ there is a period doubling bifurcation to a two cycle, followed by a frequency doubling cascade into chaos. Chaos is clearly seen since the Lyapunov number increases by two orders of magnitude. At $\Gamma_3 = 4.8$, 5.8, 6.2, and 6.4, there are tangent bifurcations to stable limit cycles. For $\Gamma_3 > 6.4$ the limit cycle remains stable all the way through $\Gamma_3 = 20$.

## VIII. CONCLUSIONS

The Zakharov equations and related PDE systems have been used to model turbulence in plasmas and fluids in which there are a large number of active degrees of freedom. In this paper, we have found a turbulence regime, described by the 1D Zakharov equations, with many active modes but with the dynamics of a system having only a few degrees of freedom. This regime is characterized by the decay of a single unstable pump Langmuir-wave mode coupled to broadened spectra of daughter Langmuir and ion-acoustic waves.

While it is tempting to simply implement a Galerkin truncation to three modes (one pump and two daughters), the justification for such a truncation must be based on the actual dynamics of the multimode (Zakharov-equation) system. Furthermore, it is not *a priori* clear which daughter modes to include in the truncation. The obvious choice is the linearly most (parametrically) unstable pair of daughter modes given the constraint of three-mode wave number matching. This condition of maximum instability is satisfied for the case of zero frequency mismatch, which corresponds to the daughter Langmuir wave at $k = k_S$ and the daughter ion-acoustic wave at $k = k_{ia}$. However, as shown in Sec. VI B 3, zero frequency mismatch ($\Delta = 0$) is a special case with one fewer degrees of freedom than the typical case. In fact, as the Zakharov-equation solutions demonstrate (cf. Table II), the multimode dynamics *do not* generally yield exact frequency matching.

The appropriate three-mode truncation is found to depend on both the shape and correlation properties of the broadened daughter-wave spectra. When the effective lumped-mode daughter waves—determined according to the analysis of Sec. IV—are used in the reduced three-mode system, the nonlinear dynamical evolution corresponds well to the dynamics of the multimode system. This *quantitative* agreement is lost when the linear ion-acoustic response operator is reduced from second to first order (the discarded degree of freedom corresponding to an off-resonance density wave). Nevertheless, *qualitative* agreement is maintained (through small adjustments in

properties of the *effective* daughter modes). This reduction in order is useful analytically because it brings our lumped-mode system into correspondence with a generalization of the dynamical system studied by WFO.

The reduced system we study here differs from that of WFO in that it allows the two daughter modes to have unequal damping rates—thereby preventing a reduction in order of the dynamical system (from four to three *real* degrees of freedom), which WFO used to simplify their analysis. The higher-order system we consider still reveals a wealth of nonlinear behaviors including transitions to and from chaos. In addition, the nonequality of the damping rates allows for bounded solutions when the frequency mismatch vanishes.

The physical parameters (e.g., driving and damping rates) used in this study were chosen to approximate those measured in the Earth's auroral ionosphere during periods of Langmuir-wave excitation. We nevertheless urge caution in the direct application of the dynamical behavior discussed here to observed Langmuir-wave turbulence. The relaxation of idealizations employed in this study may have important consequences in terms of the dynamics of the turbulence—most significantly, the one dimensionality (and consequent neglect of magnetic effects), and the restriction to a single driven mode (or, equivalently, infinite coherence length of the pump). Both of these effects will be considered in future investigations.


[1] E. N. Lorenz, Atmos. Sci. **20**, 130 (1963).

[2] J. H. Curry, Commun. Math. Phys. **60**, 193 (1978).

[3] David A. Russell and Edward Ott, Phys. Fluids **24**, 1976 (1981).

[4] V. E. Zakharov, Zh. Eksp. Teor. Fiz. **62**, 1745 (1972) [Sov. Phys. JETP **35**, 908 (1972)]. **18**, 154 (1986).

[5] G. Pelletier, M. V. Goldman, H. T. Moon, and W. Merryfield, Physica D **18**, 154 (1986).

[6] D. L. Newman, M. V. Goldman, R. E. Ergun, and M. H. Boehm, J. Geophys. Res. **99**, 6367 (1994).

[7] D. L. Newman, M. V. Goldman, and R. E. Ergun, J. Geophys. Res. **99**, 6377 (1994).

[8] D. L. Newman, M. V. Goldman, and R. E. Ergun, Phys. Plasma **1**, 1691 (1994).

[9] J. M. Wersinger, J. M. Finn, and E. Ott, Phys. Fluids **23**, 1142 (1980).

[10] B. Hafizi, J. C. Weatherall, M. V. Goldman, and D. R. Nicholson, Phys. Fluids **24**, 145 (1982).

[11] J. C. Weatherall, D. R. Nicholson, and M. V. Goldman, Phys. Fluids **26**, 1103 (1983).

[12] P. A. Robinson and D. L. Newman, Phys. Fluids B **1**, 2319 (1989).

[13] M. V. Goldman, Rev. Mod. Phys. **56**, 709 (1984).

[14] V. E. Zakharov, in *Basic Plasma Physics*, edited by A. A. Galeev and R. N. Sudan (North-Holland, Amsterdam, 1984), Vol. 1.

[15] P. A. Robinson, D. L. Newman, and A. I. Rubenchik, Phys. Fluids B **4**, 2509 (1992).

[16] In any physical system, a wave mode will always have a finite coherence length $L_c$ corresponding to a $k$-space width $\sim L_c^{-1}$. By assuming a single pump mode, we are modeling a system in which $L_c$ is large compared to any length scale that can arise in the course of the dynamical evolution of the system.

[17] J. P. McFadden, C. W. Carlson, and M. H. Boehm, J. Geophys. Res. **91**, 12 079 (1986).

[18] M. H. Boehm, Ph.D. thesis, University of California Berkeley, 1987 (unpublished).

[19] J. P. McFadden, C. W. Carlson, M. H. Boehm, and T. J. Hallinan, J. Geophys. Res. **92**, 11 133 (1987).

[20] P. A. Robinson, D. L. Newman, and M. V. Goldman, Phys. Rev. Lett. **61**, 702 (1988).

[21] P. A. Robinson and D. L. Newman, Phys. Fluids B **2**, 2999 (1990).

[22] H. Haken, *Synergetics: An Introduction* (Springer-Verlag, New York, 1977).

[23] A. Wolf, J. B. Swift, H. L. Swinney, and J. A. Vastano, Physica D **16**, 285 (1985).

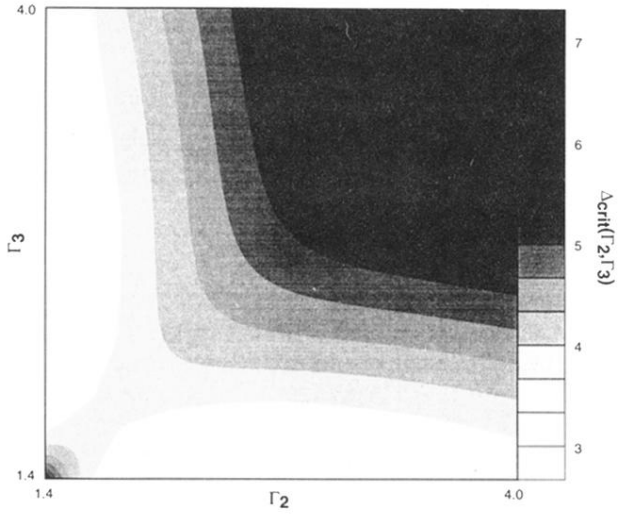


FIG. 6. Contours showing the lower bound on the value of $\Delta$ for local fixed point stability in $\Gamma_2$–$\Gamma_3$ space. Values along the diagonal ($\Gamma_2 = \Gamma_3$) correspond to Fig. 1 of WFO.